

# Physics-Informed Online Estimation of Stiffness and Shape of Soft Robotic Manipulators

Preston Fairchild<sup>®</sup>, *Graduate Student Member, IEEE*, Yu Mei<sup>®</sup>, *Graduate Student Member, IEEE*, and Xiaobo Tan<sup>®</sup>, *Fellow, IEEE* 

Abstract-Soft robots are designed to be highly compliant to reduce the risk of injury or damage to humans and the environment. This compliance can lead to large deformations when handling payloads, significantly altering the operation of the robot. The stiffness of a soft robot, actively tuned or passively influenced by inputs (e.g., pneumatic pressures), is an important state variable, yet difficult to measure directly for the control of a soft robot. In this letter we propose a novel physics-informed approach to online estimation of the stiffness and shape of a soft manipulator under a payload, based on measurements that are readily available (e.g., positions of five points on the manipulator, or the position and orientation of the tip). The same approach is also adapted for estimating the payload when the stiffness is known. The proposed method is illustrated and supported with experimental results on a soft pneumatic actuator. In particular, it is shown to produce more accurate shape estimate than a commonly adopted piecewise constant curvature (PCC) model (which cannot produce a stiffness estimate), with an average error 57% smaller than the PCC method. The stiffness values estimated are also shown to be consistent and fall within the expected physical range.

Index Terms—Soft robotic arm, modeling, online estimation, stiffness estimation.

#### I. INTRODUCTION

OFT robotics is an increasingly developing field due to the importance of safe and delicate handling of materials and interactions with humans. The softness of the baseline materials allows for utilization of soft robots in fields such as fruit harvesting and non-invasive surgery [1]. The low stiffness of soft robots, which enables safe operation, also introduces the drawback of effects such as hysteresis [2] or causing significant nonlinearities and deformation when manipulating objects or experiencing external forces. This necessitates complex models to fully capture the shape of a soft manipulator. Representing the entire shape of the robot is an important requirement for tasks such as path

Manuscript received 15 September 2023; revised 3 November 2023; accepted 20 November 2023. Date of publication 28 November 2023; date of current version 18 December 2023. This work was supported by the National Science Foundation under Grant ECCS 2024649. Recommended by Senior Editor C. Manzie. (Corresponding author: Preston Fairchild.)

The authors are with the Department of Electrical and Computer Engineering, Michigan State University, East Lansing, MI 48824 USA (e-mail: fairch42@msu.edu; meiyu1@msu.edu; xbtan@msu.edu).

Digital Object Identifier 10.1109/LCSYS.2023.3337327

planning. Some of these models discretize the soft robot (in particular, a soft robotic manipulator) into a series of points for path planning and obstacle avoidance [3], while others treat the shape of the manipulator as a continuous parametric function [4]. In order to calculate this shape, multiple methods have been developed. With known physical parameters of the soft manipulator, such as the length and stiffness, the shape can be reconstructed with a variable curvature as a Cosseratrod [5]. Other methods utilize built-in stretchable and bendable sensors to measure the curvature and reproduce the shape [6], [7]. The end orientation of the manipulator plays an important role in producing an accurate shape and representation of the manipulator. Some works utilize vision systems with markers on the tip to measure the end orientation [8], while others use electromagnetic sensors to do so [9].

While the shape of the manipulator is important for tasks such as path planning, the associated parameters that underlie the specific shape are also important for the control of the manipulator (see examples involving reinforcement learning [10] and model predictive control [11]). A key example of such parameters is the stiffness, which plays an important role in the deformation and load-bearing capability of a soft actuator [12]. The stiffness can be actively tuned via different mechanisms [13]. It can also change as a result of applied control input; for example, the pressure input values can influence the stiffness of a pneumatic actuator. Measuring the stiffness of the manipulator in real time, however, is difficult. The effects of stiffness are commonly correlated with the weight of the payload that the manipulator is handling. Various techniques have been developed to estimate the stiffness of soft manipulators. For example, the work in [14] attempts to measure the relative increase in stiffness with respect to the base stiffness to reduce the effects of an external payload but does not produce an absolute value for the stiffness. Other methods utilize the deviations from normal operations during maneuvers [15], the effects observed at different poses [16], and changes in orientations before and after attaching a payload [17]. However, these methods require a comparison of the robot at different points in time and cannot produce a real-time stiffness estimate from a single set of position measurements.

This letter aims to establish an effective and computationally efficient method for estimating the stiffness and shape of a soft robotic manipulator based on measurements easily attainable. This letter was motivated by the authors' previous work in [18]

2475-1456 © 2023 IEEE. Personal use is permitted, but republication/redistribution requires IEEE permission. See https://www.ieee.org/publications/rights/index.html for more information.

where the configuration variables (including stiffness) of the manipulator were characterized as functions of the pneumatic pressure inputs, and the coefficients of such functions are estimated based on data fitting. In particular, the stiffness value for a given set of inputs was measured manually by pulling the manipulator and measuring the resulting force and displacement. This letter, however, removes some of the assumptions involved in [18] and uses a physics-informed approach to estimate in real-time the relevant configuration variables for shape and stiffness with a small amount of data. Specifically, a model capturing the soft beam physics is incorporated to produce the shape predictions under a given set of configuration variables.

This letter has the following contributions that are not present in our previous work or in the literature. First, two methods are presented for calculating the parameters of the soft manipulator based on a single set of position measurements from the soft manipulator. The values for these parameters represent physical properties of the manipulator such as the length and actuation moment and are shown to be effective in recreating the shape of the manipulator, and thus implied to be accurate estimates. Whereas the previous work [18] used a constant curvature shape to identify parameters and then applied external loads, this letter identifies the parameters from a variable curvature shape already accounting for external payloads, making it more physically sound. Utilizing these values would allow for easier and more precise implementation of data-driven modeling and feedback control. Second, a method for estimating the stiffness value of the soft manipulator given a known payload is presented with a single frame of positional data, as opposed to previous works [15], [16], [17], [18] requiring multiple positional measurements. The proposed methods also provides physical values for the stiffness compared to a relative stiffness value as in [14]. This method is thus applicable for robotic manipulators with variable stiffness, such as those with pneumatic actuation or stiffness-tuning mechanisms. The stiffness estimate is shown to be consistent with different payload weights under the same set of control inputs. Third, a method for estimating the payload of the soft robot when the stiffness is known is presented. The proposed methods are all supported with experimental results conducted on a pneumatic actuator with payloads.

## II. APPROACH TO SHAPE MODELING AND ESTIMATION A. Variable Curvature Model and Its Computation

The piecewise constant curvature (PCC) model separates a soft robotic arm into individual segments composed of arcs of a circle. This approach is popular due to its simplicity. It is often valid for typical actuation mechanisms in soft robotics, such as soft manipulators actuated by cables or pneumatic pressure, when gravity or external forces can be ignored. Due to the actuation effect being uniform along a given section of the robot, one can assume that the generated actuation moment is uniform, which would result in a constant curvature for that section, assuming a soft robot with a

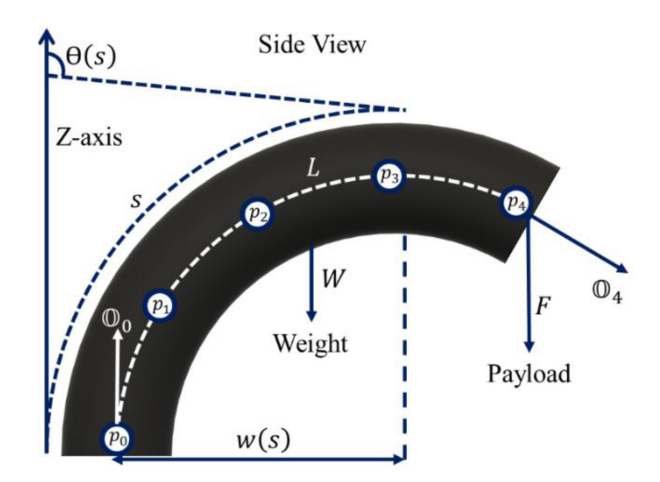


Fig. 1. Parameters of the soft robot bending from side view of the bending plane.

consistent bending stiffness, *EI*, along the length, such as in a cylindrical manipulator. Specifically, one has:

$$k(s) = \frac{\mathrm{d}^2 w}{\mathrm{d}x^2} = \frac{M(s)}{EI}, \ s \in [0, \ L],$$
 (1)

where k(s) describes the curvature at point s, s is the arclength parameter, L is the total length of the section,  $d^2w/dx^2$  describes the second derivative of the deflection, w, with respect to the initial length coordinate, x, M(s) is the moment at point s, and EI is the bending stiffness of the manipulator defined by Young's Modulus, E, and the second moment of area, I. As evident from (1), with a constant actuation moment  $M(s) = M_0$ , the curvature will be constant in the absence of other forces. This assumption is substantiated with further results presented in Section IV-A.

When gravity and external forces are incorporated into the total moment the soft manipulator can be treated as an arc with variable curvature as implied by (1). To describe the shape of the manipulator, the following information needs to be available:  $p_0$  and  $\mathbb{O}_0$ , representing the position and orientation at the base, respectively; the bending direction  $\varphi$ ; w(0), indicating the initial deflection at  $p_0$  which can be assumed to be 0; M(s), EI, and L. These values collectively form the parameters of the manipulator.

Some of the aforementioned variables, such as  $p_0$  and  $\mathbb{O}_0$ , can be assumed to be known. Other variables, such as EI and L, are constants that need to be identified. M(s) consists of the moment generated by actuation (independent of s) and the moments generated by external forces. For example, moments produced by a payload,  $M_P(s)$ , and by the weight of the manipulator itself,  $M_w(s)$ , are described as follows:

$$M_P(s) = F\sin(\theta(L))[w(L) - w(s)] \tag{2}$$

$$M_w(s) = \int_s^L \frac{W}{L} \sin(\theta(s)) [w(L) - w(s)] ds, \tag{3}$$

$$\theta(s) = \int_0^s k(s)ds \tag{4}$$

$$w(s) = \int_0^s \sin(\theta(s))ds. \tag{5}$$

In these equations, F is the weight of a point payload,  $\theta(s)$  is the bending angle relative to the base at point s along the manipulator, and W is the weight of the manipulator, as illustrated in Fig. 1. Using (4), it is possible to reconstruct the 3D shape of the manipulator along the arclength as follows:

$$\frac{dx}{ds} = \cos(\varphi)\sin(\theta(s)),$$

$$\frac{dy}{ds} = \sin(\varphi)\sin(\theta(s)),$$

$$\frac{dz}{ds} = \cos(\theta(s)).$$
(6)

The external moments change the curvature of the manipulator, thereby affecting its bending. Simultaneously, the moments themselves are also affected by the bending of the manipulator. In order to circumvent this issue of circular coupling, we propose an iterative procedure for computing the shape, for a given uniform actuation moment, when subject to weight or external forces. First, one computes the constant curvature shape corresponding to the actuation moment, assuming the absence of the weight or external forces. Then, given the previously obtained shape, one evaluates the external moments due to the weight or external forces, which are incorporated to produce updated curvature function as in (1). This process can be repeated iteratively until it converges to a stable curvature function. This convergence will occur when the overall bending angle,  $\theta(L)$ , does not exceed 180° during the iteration, which ensures that the moments generated in (2) and (3) are always positive. This condition can be achieved under sufficiently high stiffness.

#### B. Parameter Estimation

The goal of the estimation is to find values for the actuation moment  $M_0$ , the bending direction  $\varphi$ , the stiffness EI, and the actuator length L, so that the model shape, evaluated from (1)–(6), matches the available measurements under a given set of control inputs and external forces. We here write the model parameters as  $X = (M_0, \varphi, EI, L)$ .

First, we consider the case of measuring the positions of  $K_1 \geq 2$  points on the manipulator, denoted as  $S_1 = (p_1, \ldots, p_{K_1})$ , with  $p_i \in \mathbb{R}^3$ ,  $i = 1, \ldots, K_1$ , representing the measured position of the manipulator at arclength  $s_i > 0$ . These points will be used for estimating the model parameters, X. Let  $\Lambda_X$  denote the manipulator shape represented by X, through the modeling process described in the preceding subsection, i.e.,  $\Lambda_X(s)$  denotes the model-predicted 3D position of the point with arclength s. The optimal parameter  $X^*$  is then found through:

$$X^* = \arg\min_{x} \sum_{i=1}^{K_1} c_i \|\Lambda_X(s_i) - p_i\|_2$$
 (7)

where  $c_i > 0$  represents the weight placed on the error at the *i*-th location—for example, one would put larger weight on points closer to the base since they would have larger influences on the manipulator configuration. In our later experiments, the points are uniformly spaced along the manipulator,  $s_i = \frac{iL}{k_1}$  and we use  $c_i = \frac{1}{iL}$ .

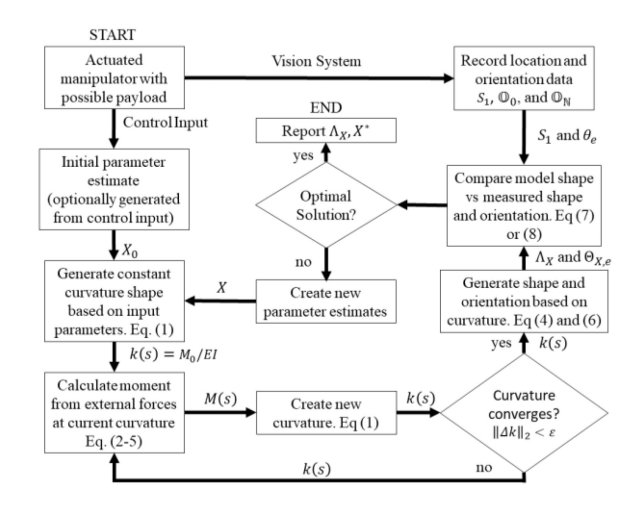


Fig. 2. Flowchart of the proposed method.

Next, we consider the case of only measuring the endpoint position  $p_e$  and bending angle  $\theta_e$  at arclength  $s_e$ . Let  $\Theta_{X,e}$  denote the model-predicted endpoint bending angle. The optimal parameter  $X^*$  is then found through:

$$X^* = \arg\min_{X} \|\Lambda_X(s_e) - p_e\|_2 + C |\Theta_{X,e} - \theta_e|$$
 (8)

where C is chosen to weigh the importance of the two cost terms. One potential value for C is  $L/2\pi$ , normalizing the maximum error of the two values. In this letter, the method with measurements of points along the manipulator (i.e., (7)) is denoted as the *full points* method, while the approach using the tip position and orientation (i.e., (8)) is termed the *end orientation* method. A flowchart depicting these processes is shown in Fig. 2. To evaluate the accuracy of the estimated manipulator shape, we use an error formula analogous to (7), where the used measurements (ground truth) could differ from those used in parameter estimation.

The methods presented above rely on estimates of the parameters to generate the prediction of positions for a set of points of interest, for a given set of control inputs and payload. If one assumes that the stiffness is known under a given set of control inputs (for example, estimated via the aforementioned methods using (7) or (8)), the same approach can be adapted to estimate the payload, where the set of parameters to be estimated will include the payload value instead of the stiffness.

#### III. EXPERIMENTAL SETUP

In this section the experimental setup used to validate the model and parameter estimation is discussed. The soft robot utilized for these experiments is a single-segment, three chamber pneumatic soft manipulator with a diameter of 4 cm, a length of 20 cm, and a weight of 200 g. The manipulator was placed within an Opti Track motion tracking system with 10 cameras arranged to observe the entire surface of the manipulator during actuation and capable of accurately tracking the shape of the robot during actuation to  $\pm 0.5$  mm.

The robot was equipped with four sets of motion tracking markers to calculate the set of ground truth points  $(K_1 = 4)$ .



Fig. 3. Experimental setup of the soft manipulator.

TABLE I
MODEL PROCESSING TIME

Method	Mean (s)	Max (s)	STD (s)
Proposed Full Points	0.236	0.776	0.121
End Orientation	0.123	0.342	0.033
Full Point CC	0.025	0.041	0.005

The markers were placed around the circumference of the robot with the plane formed by the markers used to calculate the orientations of the base and tip points. Each point was transformed so that the base of the manipulator was placed at the origin, and the initial orientation was aligned with the z-axis. During experiments, the robot was actuated using 15 unique pressure combinations across the three chambers to collection motion tracking data with and without any payload ranging from 150 g to 230 g in 20 g increments, resulting in a total of 6 datasets for each pressure control input. For this initial data set, we processed the data to calculate the positional percent error of the manipulator from all points, as defined by the summation in (7), along with the stiffness estimate. Subsequently, an additional dataset was obtained at the same pressure control inputs with payload weights varying from 140 g to 240 g that were not included in the initial dataset. This second set of data was used to evaluate the weight estimation of the model shown in Section IV-C. The experimental setup is visually represented in Fig. 3.

The data processing was conducted using the fmincon function in MATLAB to perform the minimization process. The processing was executed on a Windows desktop equipped with 16GB of RAM and an Intel i5-7600K processor. The proposed methods are compared to two baseline models. The first is the PCC model (which degenerates to CC for a single segment) that attempts to minimize the same cost function as the full points method from the summation in (7). The second is a PCC model that only has knowledge of the endpoint and uses the unique set of parameters to reach this point. The calculation times of the compared methods are shown in Table I. The endpoint CC has a trivial solution and is solved nearly instantaneously thus not included. It is evident from the processing times that the full points CC method is significantly faster than the two proposed methods as it does not iteratively calculate the moment. Between the two proposed methods, the end orientation method is faster than the full points method. This disparity is attributed to the reduced complexity of the minimization function in the end orientation method. However, both processes are sufficiently fast to be practical for online applications.

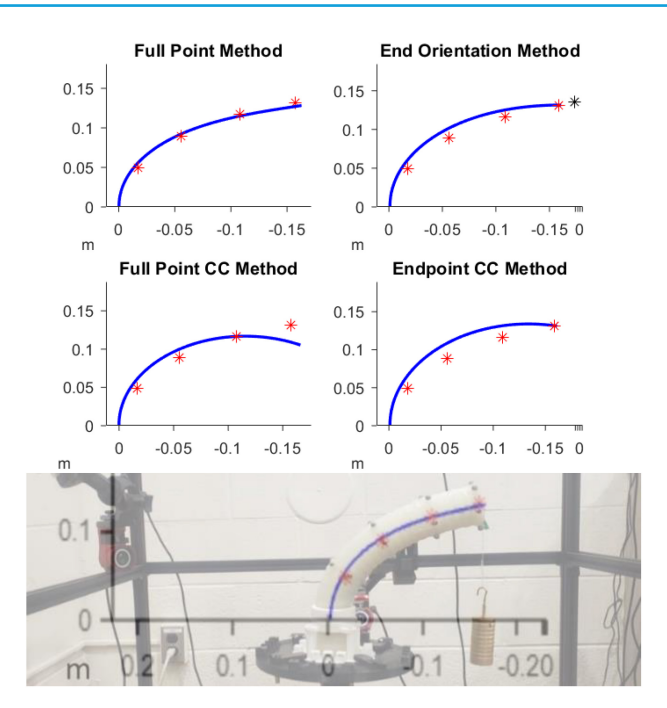


Fig. 4. (Top) Reconstructed shape in blue line vs measured points in red stars and end orientation as line between the end red and black star. (Bottom) Full point method overlayed on soft robot.

TABLE II
SHAPE ESTIMATION PERCENT ERRORS

Model	Mean	Max	STD	No Load
	Error	Error		Error
Full Points	2.94%	5.17%	0.68%	2.06%
End Orientation	5.47%	9.07%	1.49%	2.96%
PCC All Points	6.84%	10.4%	2.05%	3.40%
PCC End Point	7.70%	12.6%	2.55%	3.50%

#### IV. RESULTS

#### A. Shape Estimation Results

The results from the experimental setup described in Section III are discussed here. The effectiveness of each method to produce an accurate shape reconstruction is calculated through the summation in (7) and is given in Table II. A set of reconstructed shapes and the corresponding physical bending shape from an experiment with a payload of 230 g are shown in Fig. 4.

The data demonstrates promising results regarding the effectiveness of the proposed methods. Both methods outperformed the PCC model in shape estimation. When comparing the proposed models to their corresponding PCC models with knowledge of the same points, the full points method exhibited a 57% improvement over the PCC model, while the end orientation method showed an average improvement of 41%. These results are similar to those presented in [14] where implementation of stiffness in the model reduced the error of the open-loop control by up to 50%. It is also promising that, for every single dataset, the proposed methods consistently outperformed the PCC methods. The proposed methods show similar results to soft robots equipped with internal sensors

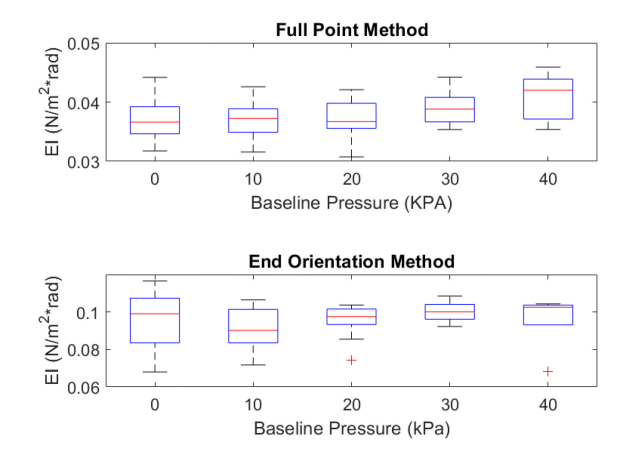


Fig. 5. Stiffness measurements under identical baseline (minimum) pressure inputs.

such as those presented in [6] with a 4.45% tip error and [7] with  $\approx$ 7% end angle error. Additionally, the error under no load also acts as validation for the assumption that the manipulator follows the PCC assumption without any external forces. Although the effects of gravity on the manipulator are still present under no load, the moment generated by gravity is relatively small compared to that induced by a payload. Since the errors for the PCC model are significantly smaller than those observed under load conditions, they can be considered as effective representations of the shape and contribute to validating the assumption.

#### B. Stiffness Estimation Results

The stiffness estimation of the manipulators was also calculated for every datapoint. Unlike the shape estimation, there are no ground truth values to compare the estimations to as the stiffness of the manipulator is variable based on the pneumatic pressure input. A theoretical stiffness value can be computed based on the design of the manipulator and the material properties, but it does not consider the effect of pneumatic inputs. Instead of comparing against an absolute stiffness value, the stability of stiffness estimate across different payloads is observed. If the stiffness estimate is accurate, it should remain relatively consistent across various payloads with the same actuation input. Therefore, to evaluate the effectiveness of the model, the variances in the stiffness estimates are compared. Additionally, when the robot is not carrying a payload, the effects of the external moments are minimal relative to loaded conditions. Consequently, the stiffness estimates for the robot without a payload are highly sensitive to measurement values, making it impractical to obtain an accurate stiffness measurement unless the manipulator is carrying a payload. Therefore, we consider only the datasets where the robot is handling a payload. The results of these estimates are presented in Table III, with a representation of the measured stiffness values under different minimum baseline pressure inputs of the three chambers presented in Fig. 5.

The relative variance in the stiffness values is quite low for the tested data. Additionally, for the full points method, there is a general increase in the stiffness values as the baseline

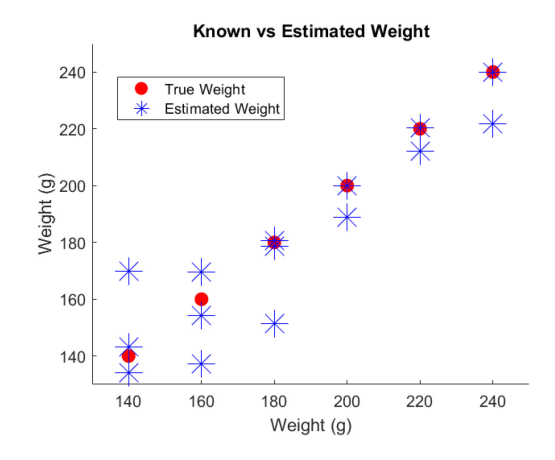


Fig. 6. Applied weights (red circles) vs estimated weights (blue stars).

### TABLE III STIFFNESS ESTIMATION RESULTS

mN/(m <sup>2</sup> *rad)	Avg STD	Max STD	Relative STD
Full Points	2.9	4.2	7.71%
End Orientation	6.7	19.5	17.76%

pressure increases, as expected. This helps confirm that the model provides an accurate estimation for the stiffness. The full points method has a lower stiffness estimate than the end orientation method and the theoretical base stiffness of the manipulator. This can be attributed to the manipulator not being held completely rigidly in place and thus having some initial bending angle that affects the points near the base. Since the full points method is more sensitive to the error near the base, it lowers the stiffness to compensate.

#### C. Payload Estimation Results

The final set of data was used to estimate the payload for the manipulator with a given stiffness. The same control inputs from the first set of data were used, and the stiffness estimates from the initial datasets were employed to establish stiffness values for the payload estimation. Due to higher variance in the end orientation method, only the full points method was utilized for weight estimation. The resulting payload estimates exhibited an average error of 9.7 g with a maximum error of 29.9 g and an average percent error of 4.97% of the total weight. A plot of the known vs estimated payload across the 15 experiments is shown in Fig. 6.

The weight estimation yields satisfactory results, especially considering that the stiffness estimate is derived from previous experiments. The estimates present similar results to those in [15], with payloads sorted in ranges of 50 g, and present better results than those in [17] which had a 20% relative error in payload estimation. With the full points model, it becomes feasible to obtain a reasonable payload weight estimate based on the shape alone.

#### V. CONCLUSION

We presented a new physics-informed approach to estimating the parameters of a soft manipulator to reproduce its shape. It was built upon a validated assumption that the manipulator

follows a constant curvature shape in the absence of external forces as an initial state for an iterative moment calculation, and external forces will cause a change in curvature relative to their generated moments. Two methods were proposed for parameter estimation: one leveraging information from multiple ground truth points on the robot, and another utilizing only the tip position and orientation. Both methods also allow for estimation of the stiffness of the manipulator with a known payload, and for the full points method, estimation of the payload of the robot under actuation inputs with known stiffness. The methods were validated with experimental results that showcased the efficacy of the models compared to the constant curvature model. While the end orientation method has a faster processing time, it is outperformed by the full points method in all other metrics. The full points method not only produces the most accurate shape, but also delivers lowvariance stiffness estimates and relatively accurate estimates of the payload. This method is highly preferable in scenarios where multiple positional values can be measured on the soft robot.

While both methods performed better than the constant curvature model, the end orientation method lags significantly behind the full points method, which ideally should produce similar results. One possible reason for this discrepancy lies in the variance in positional data, which can lead to substantial variations in orientation measurements generated by the planes formed by these points, even with small changes in position.

Future work will include rigorous investigation into the specific conditions and rates of convergence for the iterative moment calculation, for a given set of configuration variables. Additional work involving further integration of the models into soft robots is also possible. In this letter, only external moments directly impacting or opposing the bending direction were examined, as in the case of a single segment oriented vertically. External moments not applied in the plane of bending could be incorporated as some stretching and shearing deformations on the soft robot, such as those in a Cosserat Rod. Additionally, tests could be done in realtime to validate the efficacy of the model to work in a more dynamic environment. The model could also be implemented for the case of multiple segments on a soft robot, where each attached segment treats its adjacent segment as a set of external moments and payloads.

#### **ACKNOWLEDGMENT**

The authors would like to acknowledge Noah Shepard for his help with the prototyping of the soft robotic manipulator used for experimental validation.

#### REFERENCES

- [1] M. Runciman, A. Darzi, and G. P. Mylonas, "Soft robotics in minimally invasive surgery," *Soft Robot.*, vol. 6, no. 4, pp. 423–443, 2019.
- [2] M. T. Thai, P. T. Phan, T. T. Hoang, H. Low, N. H. Lovel, and T. N. Do, "Design, fabrication, and hysteresis modeling of soft microtubule artificial muscle (SMAM) for medical applications," *IEEE Robot. Autom. Lett.*, vol. 6, no. 3, pp. 5089–5096, Jul. 2021.
- [3] S. Mbakop, G. Tagne, O. Lakhal, R. Merzouki, and S. V. Drakunov, "Path planning and control of mobile soft manipulators with obstacle avoidance," in *Proc. 3rd IEEE Int. Conf. Soft Robot. (RoboSoft)*, 2020, pp. 64–69.
- [4] P. R. Fairchild, V. Srivastava, and X. Tan, "Efficient path planning of soft robotic arms in the presence of obstacles," in *Proc. Model. Estimat. Control Conf.*, Austin, TX, USA, 2021, pp. 586–591.
- [5] D. C. Rucker and R. J. Webster, "Statics and dynamics of continuum robots with general tendon routing and external loading," *IEEE Trans. Robot.*, vol. 27, no. 6, pp. 1033–1044, Dec. 2011.
- [6] J. So et al., "Shape estimation of soft manipulator using stretchable sensor," Cybord Bionic Syst., vol. 2021, Apr. 2021, Art. no. 9843894.
- [7] D. Lunni, G. Giordano, E. Sinibaldi, M. Cianchetti, and B. Mazzolai, "Shape estimation based on Kalman filtering: Towards fully soft proprioception," in *Proc. IEEE Int. Conf. Soft Robot. (RoboSoft)*, Livorno, Italy, 2018, pp. 541–546.
- [8] L. Lindenroth et al., "Stiffness-based modelling of a hydraulically-actuated soft robotics manipulator," in *Proc. IEEE/RSJ Int. Conf. Intell. Robots Syst. (IROS)*, 2016, pp. 2458–2463.
- [9] Y. Chen, L. Wang, K. Galloway, and I. Godage, "Modal-based kinematics and contact detection of soft robots," *Soft Robot.*, vol. 8, no. 3, pp. 298–309, 2021.
- [10] T. G. Thuruthel, E. Falotico, F. Renda, and C. Laschi, "Model-based reinforcement learning for closed-loop dynamic control of soft robotic manipulators," *IEEE Trans. Robot.*, vol. 35, no. 1, pp. 124–134, Feb. 2019.
- [11] F. A. Spinelli and R. K. Katzchmann, "A unifed and modular model predictive control framework for soft continuum manipulators under internal and external constraints," in *Proc. IEEE/RSJ Int. Conf. Intell. Robots Syst. (IROS)*, Kyoto, Japan, 2022, pp. 9393–9400.
- [12] M. T. Gillespie, C. M. Best, and M. D. Killpack, "Simultaneous position and stiffness control for an inflatable soft robot," in *Proc. IEEE Int. Conf. Robot. Autom. (ICRA)*, Stockholm, Sweden, 2016, pp. 1095–1101.
- [13] Y. Mei, P. Fairchild, V. Srivastava, C. Cao, and X. Tan, "Simultaneous motion and stiffness control for soft pneumatic manipulators based on a Lagrangian-based dynamic model," in *Proc. Amer. Control Conf.*, Sand Diego, CA, USA, 2023, pp. 145–152.
- [14] J. Lai, B. Lu, and H. K. Chu, "Variable-stiffness control of a dual-segment soft robot using depth vision," *IEEE/ASME Trans. Mechatronics*, vol. 27, no. 2, pp. 1034–1045, Apr. 2022.
- [15] D. Bruder, X. Fu, R. B. Gillespie, C. D. Remy, and R. Vasudevan, "Koopman-based control of a soft continuum manipulator under variable loading conditions," *IEEE Robot. Autom. Lett.*, vol. 6, no. 4, pp. 6852–6859, Oct. 2021.
- [16] Y. Toshimitsu, K. W. Wong, T. Buchner, and R. Katzchmann, "SoPrA: Fabrication & dynamical modeling of a scalable soft continuum robotic arm with integrated proprioceptive sensing," in *Proc. IEEE/RSJ Int. Conf. Intell. Robots and Systems (IROS)*, Prague, Czech Republic, 2021, pp. 653–660.
- [17] X. Chen, D. Duanmu, and Z. Wang, "Model-based control and external load estimation of an extensible soft robotic arm," *Front. Robot. AI*, vol. 7, Jan. 2021, Art. no. 586490.
- [18] P. Fairchild, N. Shephard, Y. Mei, and X. Tan, "Semi-physical modeling of soft pneumatic actuators with stiffness tuning," ASME Lett. Dyn. Syst. Control, vol. 3, no. 4, pp. 1–6, Nov. 2023. [Online]. Available: https://doi.org/10.1115/1.4064090